Geopolymerization of halloysite via alkali-activation: Dependence of microstructures on precalcination

7 authors, including:

Zhang Baifa
Chinese Academy of Sciences
7 PUBLICATIONS **4** CITATIONS

SEE PROFILE

Peng Yuan
Chinese Academy of Sciences
178 PUBLICATIONS **6,405** CITATIONS

SEE PROFILE

Yun Li
Chinese Academy of Sciences
13 PUBLICATIONS **32** CITATIONS

SEE PROFILE

Liang liang Deng
Chinese Academy of Sciences
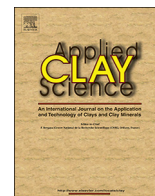**22** PUBLICATIONS **238** CITATIONS

SEE PROFILE

Some of the authors of this publication are also working on these related projects:

Project   The structural stability and potential applications of allophane and imogolite View project

Project   utilization of rare earth tailings View project

Research Paper

Geopolymerization of halloysite via alkali-activation: Dependence of microstructures on precalcination

Baifa Zhang[a,b], Haozhe Guo[a,b], Peng Yuan[a,b,*], Yun Li[a,b], Qiang Wang[a,b], Liangliang Deng[a,b], Dong Liu[a,b]

[a] CAS Key Laboratory of Mineralogy and Metallogeny, Guangdong Provincial Key Laboratory of Mineral Physics and Materials, Guangzhou Institute of Geochemistry, Institutions of Earth Science, Chinese Academy of Sciences, Guangzhou 510640, China
[b] University of Chinese Academy of Sciences, Beijing 100049, China

ABSTRACT

Halloysite has a chemical composition very similar to that of kaolinite, but it possesses a special nanotubular structure and surface reactivity. This work focuses on the geopolymerization of halloysite via alkali-activation, and investigates the effects of precalcination temperatures ranging from 450 °C to 1000 °C on the microstructures and mechanical properties of halloysite-based geopolymer. The products obtained were characterized using a combination of techniques including X-ray diffraction, Fourier-transform infrared spectroscopy, scanning electron microscopy, N_2 physisorption analysis, and nuclear magnetic resonance. The results show that halloysite underwent minimal structural changes when calcined at 450 °C, and its alkali-activation product showed poor mechanical properties due to the formation of hydrosodalite with a porous structure. The dehydroxylation that occurred at calcination temperatures between 650 °C and 850 °C could improve the reactivity of halloysite with alkaline solution. The formation of geopolymer with a compact structure resulted in increased compressive strength. When halloysite was calcined at 1000 °C, geopolymerization also occurred, but to a lesser extent because of the formation of nanosized γ-Al_2O_3. This resulted in a decreased compressive strength in the product. These results indicate that the microstructures and properties of halloysite-based geopolymers are greatly dependent upon the precalcination of halloysite and that the optimal temperature is around 750 °C to ensure a high degree of dehydroxylation with high reactivity, which is favorable for geopolymerization.

1. Introduction

Geopolymer is an inorganic polymeric material that consists of cross-linked tetrahedral [AlO_4] and [SiO_4] units with hydrated alkali metal cations (Duxson et al., 2007). Owing to their three-dimensional network structure, geopolymeric materials possess high durability, good chemical resistance, and excellent mechanical properties (Duxson et al., 2007; Temuujin et al., 2009; Zhang et al., 2015; Ribeiro et al., 2016), which make them highly useful in applications such as heavy metal immobilization, infrastructure construction, and composite manufacturing (Provis and Bernal, 2014; Joussein et al., 2019). Geopolymer has attracted considerable research attention in recent years as a potential alternative to ordinary Portland cement (OPC), because the manufacturing process for geopolymer involves lower energy consumption and fewer CO_2 emissions (Mclellan et al., 2011; Shi et al., 2011; Font et al., 2018). Normally, geopolymer can be synthesized by

activating aluminosilicate precursors with a highly alkaline solution, followed by curing at an ambient or elevated temperature (Hanjitsuwan et al., 2014; Zhang et al., 2016; Monneron-Gyurits et al., 2018).

Generally, materials with sufficient amounts of reactive alumina and silica are potential sources for geopolymer synthesis (Belmokhtar et al., 2018; Bumanis et al., 2019). For example, clay minerals are frequently used as precursors in geopolymerization due to their high reactivity (Hu et al., 2016; Dietel et al., 2017; Marsh et al., 2019). Kaolinite ($Al_2(OH)_4Si_2O_5$), a 1:1 dioctahedral clay mineral with unit layers consisting of a silica tetrahedral sheet and an alumina octahedral sheet, is one of the most commonly used aluminosilicate precursors in geopolymer preparation (Zhang et al., 2012b; Zhang et al., 2013; Liew et al., 2016; Selmani et al., 2017). Thermal pretreatment is usually used to enhance the reactivity of kaolinite (Wan et al., 2017a; Tchadjie and Ekolu, 2018) because the mechanical strength of geopolymer prepared using unheated kaolinite is low. Typically, the optimal precalcination
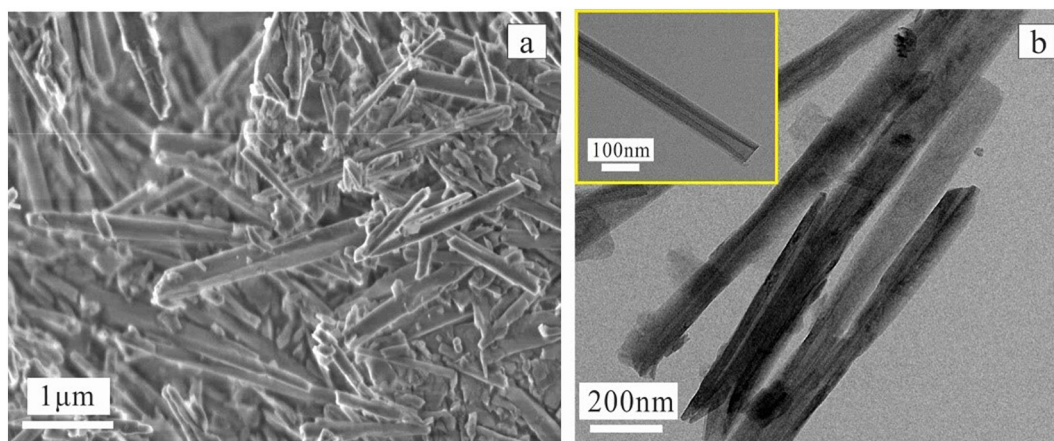
Fig. 1. SEM image (a) and TEM image (b) of Hal.

temperature of kaolinite falls in the range between 600 °C and 900 °C, which can transform the crystalline phase of kaolinite into amorphous phases of metakaolinite. (Zhang et al., 2009a; Elimbi et al., 2011; Ferone et al., 2015).

Halloysite ($Al_2(OH)_4Si_2O_5 \cdot 2H_2O$) is a hydrated polymorph of kaolinite that shows some similarities in chemical composition to kaolinite (Yuan et al., 2008; Deng et al., 2017). However, halloysite has a nanosized tubular structure that results from wrapping of the 1:1 aluminosilicate layers due to the mismatch in the oxygen-sharing tetrahedral and octahedral sheets (Joussein et al., 2005; Yuan, 2016; Wei et al., 2019). The reserve of halloysite deposits worldwide is large (Joussein, 2016) although its magnitude is smaller than that of kaolinite deposites worldwide. Notably, due to the lack of knowledge on halloysite historically, some halloysite ores were mistaken as kaolinite ores. Some advantages in the properties of halloysite over kaolinite are as follows. Halloysite has a higher specific surface area and a lower structural ordering than plate-like kaolinite (Joussein et al., 2005; Hollanders et al., 2016). And halloysite exhibits less chemical stability than kaolinite, which yields higher reactivity with alkaline solutions (White et al., 2012). Previous studies (Yuan et al., 2006; Yuan, 2016) have reported that calcined halloysite has morphological and textural characteristics unlike those of kaolinite. Dehydroxylation of halloysite occurs at ~500 °C to ~900 °C. Within this range, the structure changes dramatically, while the morphology and porosity change little. When halloysite is heated to ~1000 °C, the nanotubes become distorted and begin to break down, which causes a decrease in porosity. Furthermore, nanosized γ-Al_2O_3 is formed at this temperature, whereas mullite and cristobalite are formed at the calcination temperature of ~1400 °C (Yuan et al., 2012).

Halloysite has been used as an additive to improve the properties of cement and concrete (Farzadnia et al., 2013; Owsiak and Soltys, 2015; Yuan et al., 2015; Zapala-Slaweta, 2017). In recent years, it has also been used in the preparation of geopolymer products. Barrie et al. (2015) prepared geopolymer using halloysite-rich clay, volcanic glass, and mine tailings and found that calcined halloysite was the main active component during geopolymerization, which improved compressive strength. Zhang et al. (2012a) studied the influence of halloysite as a second mineral component present in kaolinite on the preparation of metakaolin-based geopolymer and found that halloysite-containing kaolinite shows higher geopolymerization reactivity than purer metakaolin. From the above studies, it is likely that halloysite exhibits a higher reactivity with an alkaline solution than kaolinite. However, studies of halloysite-based geopolymer are far less reported than those for other precursors such as kaolinite, illite, and fly ash (Buchwald et al., 2009; Hu et al., 2016; Duan et al., 2017). In addition, the calcination-induced changes in structure, morphology, porosity and surface activity of halloysite are different from those of kaolinite (Yuan

et al., 2016), which may show different reaction behavior during alkali-activation. However, in most studies, the reaction mechanism of alkali-activated halloysite is regarded as analogous to that of kaolinite.

In this work, we investigated the use of calcined halloysite in the preparation of geopolymer via alkali-activation. The effects of calcination temperatures of halloysite on the degree of geopolymerization, the composition and microstructure of the alkali-activation product, and the compressive strength of the products were studied. The aim of this work was to gain a better understanding of the geopolymerization of calcined halloysite during the process of alkali-activation. Different analytical technologies, including inductively coupled plasma optical emission spectrometry (ICP-OES), X-ray diffraction (XRD), Fourier-transform infrared (FT-IR) spectroscopy, nuclear magnetic resonance (NMR), scanning electron microscopy (SEM) and N_2 physisorption analysis, were used to investigate the microstructures and properties of alkali-activation products of calcined halloysite.

2. Materials and characterization

2.1. Materials

Halloysite (Hal) was provided by I-Minerals Inc., USA. The chemical composition of Hal, as measured by X-ray fluorescence (XRF), is given as the percentage by mass of the respective oxides: Al_2O_3 (37.80%), SiO_2 (46.00%), Fe_2O_3 (0.72%), K_2O (0.30%), MgO (0.13%), CaO (0.07%), Ti_2O (0.07%), and loss on ignition (14.90%). The SEM and TEM images (Fig. 1) illustrate that the Hal possesses a tubular shape. The transparent central areas (insets of Fig. 1b) indicate that the Hal nanotubes are hollow. The specific surface area of the Hal as determined by BET method was 28.29 m^2/g.

As reported in previous studies (Yuan et al., 2015), calcination below 500 °C results in slight structural changes of halloysite. Dehydroxylation with a step-wise process occurred at calcination temperatures between 500 °C and 900 °C (White et al., 2010). Nanosized γ-Al_2O_3 was formed when halloysite was calcined at 1000 °C. In addition, 2 h calcination was sufficient to result in the structural changes for halloysite (Yuan et al., 2012). In term of this knowledge, the Hal in this study was precalcined in a muffle furnace at 450 °C, 650 °C, 750 °C, 850 °C, and 1000 °C in air for 2 h (heating/cooling rate 5 °C/min). The obtained calcined halloysites are denoted as Hal_T, where T stands for the calcination temperature. For example, Hal_{450} is the product obtained after heating Hal at 450 °C for 2 h.

On the basis of some preliminary experiments, an alkaline solution with SiO_2/Na_2O of 0.8 was selected for the synthesis of geopolymer materials. The alkaline solution was prepared by mixing chemical grade NaOH pellets (purity ≥96%) with commercial sodium water glass (original modulus of 3.33, Na_2O 8.50 wt%, and SiO_2 26.50 wt%). The
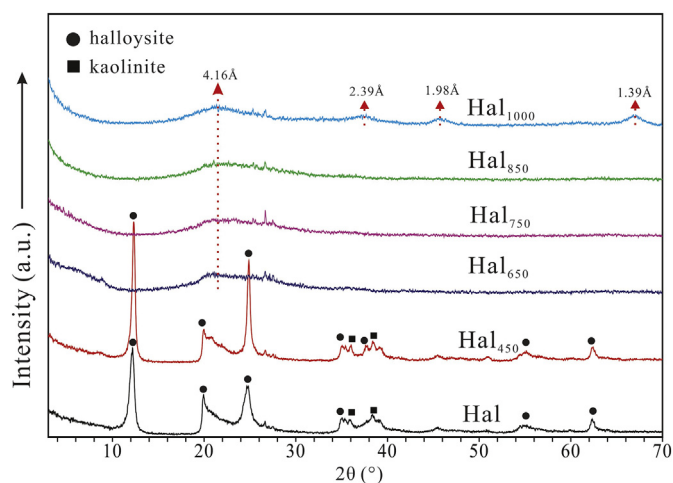
Fig. 2. XRD patterns of Hal and Hal_T.

solution was stored for 24 h before use.

2.2. Preparation of the geopolymer product

The Hal_T was mixed with alkaline solution at various liquid/solid ratios, because the minimum water requirement for workability varies for various calcination temperatures. The molar ratio of SiO_2/Al_2O_3 was set to 3.0, which has proved as an optimized condition on the basis of a series of preliminary experiments, in which various SiO_2/Al_2O_3 values had been tested. The Na_2O/Al_2O_3 ratio was set to 1.0 because sodium cations (Na^+) are required to balance equal negative charges of four-coordinated Al ($[AlO_4]^-$) in geopolymer network. The slurry was cast in plastic molds ($20 \times 20 \times 12$ mm) and covered with a thin film of polyethylene to prevent water evaporation. The molded specimens were cured at 50 °C for 48 h, and then the hardened specimens were demolded while unhardened specimens were remained in the mold. To make the samples well comparable, hardened and unhardened specimens were further cured at 80 °C for another 48 h. All demolded specimens were then stored in the plastic bags at ambient temperature until the day of the test. The obtained products are denoted as $G-Hal_T$, where T stands for calcination temperature.

2.3. Characterization methods

Alkaline leaching tests were conducted for Hal_T. 1 g of Hal_T was mixed in a shaker with 30 g of 10 mol/L sodium hydroxide solution at 25 ± 2 °C for 24 h. After centrifugation and filtration, 1 mL of clear solution was acidified with HNO_3 solution (2 wt%) to pH < 1 and diluted to 50 mL. The concentration of Si and Al in the diluted solution was then determined using an iCAP 7000 Series inductively coupled plasma optical emission spectrometry instrument (Thermo Scientific, USA).

Setting times were measured for each mixture paste. For geopolymeric pastes, setting is a process of transformation from scattered concentrated paste to connected and strengthened product of particles and the setting time means the time of the development from a plastic state to a solid state, which can be divided into initial setting and final setting time (Khan and Ullah, 2004). The Hal_T-based pastes were prepared by mixing the Hal_T and alkaline solution, and the setting times were tested using a Vicat apparatus according to the ASTM C191 standard test method.

Unconfined compression tests of alkali-activation products cured at the ages of 7 d and 28 d were performed on a YAW-300D Compression Resistance Tester (LiXian, Zhejiang) with a loading rate of 0.5 N/s.

The XRD patterns were collected by Bruker D8 Advance diffractometer (Mannheim, Germany), operating at 40 kV and 40 mA

using CuKα radiation. The specimens were investigated from 3° to 70° (2θ) with a scanning speed of 3°/min.

The FTIR spectra were recorded on a Bruker Vertex 70 spectrometer (Karlsruhe, Germany). The products were mixed with 0.8 mg of sample and 80 mg of KBr and powdered finely before the mixture was pressed the mixture into a disk. All spectra were collected in the range of 4000 to 400 cm^{-1} at a resolution of 4 cm^{-1} with 64 scans.

The SEM micrographs and energy-dispersive X-ray (EDX) spectroscopy results were obtained using an SU8010 field-emission scanning electron microscope (FESEM, Hitachi, Japan) at an accelerating voltage of 15 kV. The products were first anchored tightly on the surface of the conducting tape and then coated with a platinum layer before being transferred to the microscope.

Measurements of pore size distribution and the total pore volume were carried out using a Micromeritics ASAP 2020 instrument (Micromeritics Co., Norcross, USA) for N_2 physisorption analysis at liquid-nitrogen temperature (−196 °C). Before measurements, the products were outgassed at defined temperatures for 24 h at 393 K at the degassing port. The total pore volume was obtained from N_2 uptake at a relative pressure of 0.97.

Solid-state ^{29}Si cross-polarization magic-angle-spinning (CP/MAS) NMR spectra and ^{27}Al MAS NMR spectra were recorded on a BRUKER AVANCE III600 spectrometer. For ^{29}Si CP/MAS NMR spectra, the magnetic field strength was 14.1 T with a resonance frequency of 119.2 MHz and was recorded using a contact time of 6 ms, a π/2 pulse length of 2.3 μs, a recycle delay of 2 s and a spinning rate of 10 kHz. For ^{27}Al MAS NMR spectra, the magnetic field strength was 14.1 T with a resonance frequency of 119.2 MHz and was recorded using a small-flip angle technique with a pulse length of 0.5 μs (< π/12), a recycle delay of 1 s and a spinning rate of 14 kHz. The chemical shifts of ^{27}Al and ^{29}Si were given in ppm referenced to 1 mol/L $Al(NO_3)_3$ and tetramethylsilane (TMS), respectively.

3. Results and discussion

3.1. Changes in structure and reactivity of Hal under heating

3.1.1. Changes in structure of Hal under heating

Fig. 2 shows the XRD patterns of Hal and Hal_T. In the XRD patterns of Hal and Hal_{450}, the reflection at 12.2°(2θ) was indexed as halloysite with a d_{001} of 7.25 Å. The XRD pattern of Hal_{450} was similar to that of Hal, which indicated that no noticeable structural change occurred in the halloysite when it was calcined at 450 °C. However, in the XRD patterns of Hal_{650}, Hal_{750}, and Hal_{850}, all characteristic peaks disappeared and a major broad reflection centered at about 21.1°(2θ) (with d spacing of 4.16 Å) appeared because of dehydroxylation (Yuan et al., 2012). This demonstrated that the halloysite crystal structure has been destroyed and an amorphous phase has been formed after calcining at 650 °C to 850 °C. In the XRD pattern of Hal_{1000}, aside from the broad reflection centered at about 21.1°(2θ) (with d spacing of 4.16 Å), the broad reflections corresponding to d values of 2.39 Å, 1.98 Å, and 1.39 Å appeared, which can be assigned to the formation of nanocrystalline of γ-Al_2O_3 (Yuan et al., 2016b).

3.1.2. Dissolution behavior of calcined Hal in alkaline solution

A leaching test was used to determine the concentration of Si and Al dissolved from calcined Hal. The results displayed in Table 1 reflect the reactivity of calcined halloysites in alkaline medium. For Hal_{450}, the concentration of Si and Al in the leached solution was relatively low. Only 9.83% of the Si and 6.73% of the Al in Hal_{450} were dissolved. For Hal_{650}, the absolute amount of Al and Si leached out from the calcined Hal increased, significantly. The amount of Si leached from Hal_{650} was nearly six times higher than from Hal_{450}, whereas the Al leached from Hal_{650} was 1.3 times higher than from Hal_{450}. The Si and Al concentrations in the leached solution remained nearly unchanged as the calcination temperature increased from 650 °C to 850 °C. The degree of

Table 1
Concentration of Si and Al dissolved from Hal_T.

| | Hal_T | | | | |
	Hal_{450}	Hal_{650}	Hal_{750}	Hal_{850}	Hal_{1000}
Si	978 ppm	7030 ppm	7140 ppm	6945 ppm	5220 ppm
	9.83%	62.57%	63.53%	61.32%	45.99%
Al	641 ppm	972 ppm	969 ppm	962 ppm	480 ppm
	6.73%	9.35%	9.31%	9.28%	4.64%

dissolution for Si and Al was approximately 63.0% and 9.3%, respectively. However, the dissolution degree of Si and Al decreased to 45.99% and 4.64% for leaching of Hal_{1000}, respectively.

As the first step of geopolymerization, the dissolution of the precursor in the alkaline solution plays an important role in the formation of geopolymeric gels. Thermal treatment of halloysite can produce metahalloysite with higher reactivity. Thermodynamically, halloysite can be transformed into metahalloysite at the calcination temperature of 519 °C, which is lower than that of kaolinite (Frost and Vassallo, 1996; Yuan et al., 2016). At a low calcination temperature (450 °C), the halloysite retained a crystalline structure (Fig. 2), which resulted in low geopolymerization reactivity. Therefore, the release of Al and Si from Hal_{450} was low when it was attacked by alkaline reactant. It is worth noting that when calcined at 1000 °C, the concentration of Al in the leached solution decreased more dramatically than that of Si, indicating that γ-Al_2O_3 had low reactivity with the alkaline solution. The results of the leaching test suggest that heat treatment at proper temperatures (650 °C–850 °C) can improve the amount of Si and Al released from calcined halloysite.

3.1.3. Changes in setting time of calcined Hal-based pastes

Table 2 shows the initial setting time (the time required from mixing of precursors and activator to a certain plastic state) and final setting time (the time required from mixing of precursors and activator to a relatively dense solid state) of the pastes. G-Hal_{450} cannot set and harden at ambient temperature after 28d because of its low reactivity. The low dissolution of Si and Al from Hal_{450} hindered the polymerization of aluminate and silicate monomers (Wan et al., 2017a). The initial setting time decreased from 157 min to 100 min, whereas the final setting time decreased from 377 min to 221 min when the calcination temperature was increased from 650 °C to 850 °C (Table 2). It has been reported that the dehydroxylation of kaolinite calcined at temperatures between 500 °C and 900 °C is a step-wise process (White et al., 2010). Therefore, the state of disorder within the structure of metakaolinite, which guarantees the reactivity of kaolinite, increases as the temperature increases in certain ranges (Elimbi et al., 2011). However, when the calcination temperature increased to 1000 °C, the initial setting time increased sharply to > 4 d. The formation of γ-Al_2O_3 led to the decrease of active Al, which thus decreased the rate of polymerization and setting.

3.2. Compressive strength development of alkali-activated calcined Hal

Fig. 3 shows the 7 d and 28 d compressive strength of alkali-activated Hal_T. The 7 d compressive strength increased from 18.3 MPa to

Table 2
Setting time of mixture pastes.

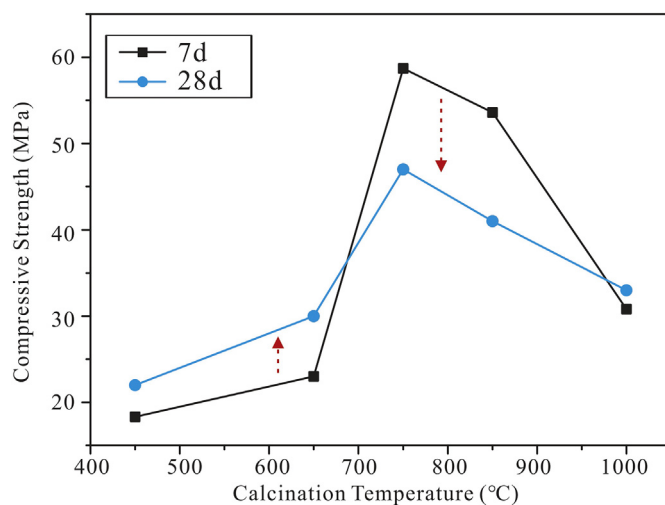| Sample	Initial Setting (min)	Final Setting (min)
G-Hal_{450}	–	–
G-Hal_{650}	157	377
G-Hal_{750}	112	262
G-Hal_{850}	100	221
G-Hal_{1000}	6750	8948

Fig. 3. Compressive strength of G-Hal_T.

58.7 MPa when the calcination temperature was increased from 450 °C to 750 °C. However, it dropped to 33.8 MPa when the calcination temperature was increased to 1000 °C. The insufficient amount of Si and Al dissolved from Hal_{450} reduced the degree of polymerization and thus negatively affected the mechanical property of the alkali-activation product. When the calcination temperature increased to 650 °C, dehydroxylation occurred, improving reactivity with the alkaline solution and thus increasing the compressive strength. However, G-Hal_{850} showed lower compressive strength than G-Hal_{750}, possibly because its rapid setting prevented continuous dissolution and thus reduced the degree of geopolymerization and compressive strength. For Hal_{1000}, the formation of γ-Al_2O_3 played a detrimental role in the formation of geopolymer and thus led to lower compressive strength.

The 28 d compressive strength of G-Hal_{450}, G-Hal_{650}, and G-Hal_{1000} increased to 21.7, 30.2, and 34.4 MPa, respectively. However, the compressive strength of G-Hal_{750} and G-Hal_{850} declined to 47 MPa and 41 MPa, respectively, at 28 d; similar results were obtained in previous studies (Zhang et al., 2009b, 2012a). Halloysite calcined at 750 °C and 850 °C possessed high reactivity with alkaline solution. When cured at high temperature, the geopolymeric paste set and hardened rapidly without sufficient reaction, coupled with the formation of large pores and excessive shrinkage; as a result, the geopolymer matrix was destroyed and negatively affected the development of compressive strength (Heide and Foldvari Heide, 2006).

3.3. Microstructure of alkali-activated calcined Hal

3.3.1. XRD results

The XRD patterns of alkali-activation products derived from halloysites calcined at various temperatures are presented in Fig. 5. The presence of hydrosodalite for G-Hal_{450} indicated that the high crystalline zeolitic nuclei content was formed when Hal_{450} reacted with the alkaline solution, which is in agreement with previous results (Duxson et al., 2007; Hounsi and Lecomte, 2013). Hydrosodalite has been synthesized using kaolinite and sodium hydroxide followed by curing at 80 °C (Marsh et al., 2018). The role of sodium silicate in this study was only to provide an alkaline environment. It appears that soluble silicate was insignificant in the alkali-activation for Hal_{450}. In addition, the unreacted halloysite can also be found according to the XRD pattern of G-Hal_{450}.

Products prepared from Hal_{650}, Hal_{750}, and Hal_{850} were XRD amorphous with one broad reflection centered at 28.3°(2θ) (with d spacing of 3.21 Å). The XRD patterns of these alkali-activation products showed no conspicuous difference in diffraction. Compared with the XRD pattern of calcined halloysite (Fig. 2), the reflection shifted to a

higher angle region after reacting with alkaline solution, demonstrating network reorganization and geopolymer formation (Duxson et al., 2007; Wan et al., 2017b; Kaze et al., 2018). There was no generation of a new crystalline phase for these products.

One broad reflection centered at 26.7°(2θ) (with d spacing of 3.32 Å) appeared for G-Hal$_{1000}$, lower than that of G-Hal$_{750}$. This phenomenon can be attributed to the lower degree of geopolymerization for G-Hal$_{1000}$ (Yuan et al., 2016). The presence of reflections corresponding to d values of 1.98 Å, and 1.39 Å in the XRD pattern indicated that nanocrystalline of γ-Al$_2$O$_3$ still remained in the product. The unreacted γ-Al$_2$O$_3$ may act as an inert filler to reinforce the structure of the geopolymeric network (Tchakouté et al., 2018). In addition, excessive alkali reacted with atmospheric CO$_2$ to form Na$_2$CO$_3$·7H$_2$O, a phenomenon known as efflorescence, which decreased the strength of G-Hal$_{1000}$ (Kani et al., 2012).

3.3.2. FTIR results

Fig. 5a displays the FTIR spectra, ranging from 400 cm^{-1} to 1600 cm^{-1}, of all alkali-activation products. G-Hal$_{450}$ showed more characteristic peaks owing to the formation of zeolitic crystalline. The absorption bands around 1029 cm^{-1} and 913 cm^{-1} were attributed to Si-O-Si stretching vibration and Al-O-H deforming vibration, corresponding to the unreacted halloysite. The band around 1453 cm^{-1} was assigned to the asymmetric stretching vibration of O-C-O bonds, which was also evident in the spectrum of G-Hal$_{1000}$, but not in the geopolymer samples. This demonstrated that less alkali took part in the geopolymerization for G-Hal$_{450}$ and G-Hal$_{1000}$. The bands at 727, 696, and 668 cm^{-1} in G-Hal$_{450}$ were attributed to stretching vibration of Si-O-T(Si, Al), while bands at 468 cm^{-1}, 433 cm^{-1} were attributed to bending vibration of T-O. The absorption band of 540 cm^{-1} was associated with the double 4-ring structure (D4R), which was the main secondary building unit of hydrosodalite (Prokof'ev and Gordina, 2014). These bands were all typical for the hydrosodalite structure (Alkan et al., 2005; Prokof'ev and Gordina, 2014; Marsh et al., 2018).

In contrast to G-Hal$_{450}$, the FTIR spectra of G-Hal$_{650}$, G-Hal$_{750}$, and G-Hal$_{850}$ showed similar characteristic peaks with broader shape, reflecting the presence of highly amorphous products (Kränzlein et al., 2018). The shoulder band at 882 cm^{-1} should be attributed to the formation of NBOs (non-bridging-oxygens), which will be more pronounced with increasing Na$^+$ concentration (Lee and Deventer, 2003). The band attributed to Si-O-T asymmetric stretching vibration between 1100 and 900 cm^{-1} plays an important role in studies of the chemistry of developing geopolymers and is often called the main band (Rees et al., 2007). For Hal$_{650}$, Hal$_{750}$, and Hal$_{850}$, their stretching band of in-plane Si-O-Si shifted toward lower wavenumbers during geopolymerization for two reasons: 1) the presence of more NBOs; 2) a reduction in the bond angle and lengthening of the Si-O-T resulting from the substitution of Al with Si (Lee and Deventer, 2003; Rees et al., 2007; Kljajević et al., 2017). Fig. 5b presents the main bands and displacement of these bands of halloysite calcined at various temperatures after geopolymerization. The left-hand-side Y axis represents the value of difference between wavenumber of Si-O-Si band for calcined halloysite and the wavenumber of Si-O-T (Al, Si) band for as-obtained geopolymer, while the right-hand-side Y axis represents Si-O-T (Al, Si) band position of geopolymers derived from halloysites calcined at different temperatures. It can be found that the main band displacement increased as the calcination temperature increased between 650 °C and 850 °C, but no distinctive difference was seen between the final wavenumbers of Si-O-T for G-Hal$_{650}$, G-Hal$_{750}$, and G-Hal$_{850}$. The main band displacement decreased sharply when the calcination temperature increased to 1000 °C, which was an indicative of a lower degree of geopolymerization (Rees et al., 2007).

For G-Hal$_{650}$ G-Hal$_{750}$, and G-Hal$_{850}$, adsorptions at 718, 581, and 439 cm^{-1} were associated with Si-O-Al^{IV} bending vibration, Al−O stretching vibration, and in-plane Si-O-Si stretching vibration, respectively. For G-Hal$_{1000}$, the broad bands of 763 and 455 cm^{-1} were

assigned to Si-O-Si symmetrical stretching vibration and Si−O bending vibration, respectively (Gao et al., 2014; Kouamo and Rüscher, 2017). A weak band at 880 cm^{-1} may belong to the bending vibration of silicate monomer (Si-OH) from unreacted silicate sodium (Li et al., 2019).

3.3.3. SEM results

Fig. 6 provides the SEM images of the alkali-activation products. G-Hal$_{450}$ showed inhomogeneous microstructure with macropores and cracks (Fig. 6a). Residual halloysite was clearly found in the matrix, which destroyed the compact structure and thus exhibited poor compressive strength. Similarly, G-Hal$_{650}$ showed loosely bound and discrete microstructure (Fig. 6b), which was responsible for the low compressive strength. By contrast, the geopolymeric matrix of G-Hal$_{750}$ and G-Hal$_{850}$ was clearly denser and more homogeneous (Fig. 6c, d), which shows good agreement with the changes in compressive strength. A compact geopolymeric matrix was formed via sufficient dissolution of calcined halloysite and polycondensation of silicate and aluminate oligomers. The Si/Al ratio of the G-Hal$_{750}$ matrix determined by EDX was 1.3 (Fig. 6f). Fig. 6e shows that G-Hal$_{1000}$ had two different morphologies: geopolymer with homogeneous microstructure, surrounded by prism-shaped, crystal-like particles. The Si/Al ratio of the geopolymeric matrix from G-Hal$_{1000}$ was 1.5 (Fig. 6f), which was higher than that of G-Hal$_{750}$, indicating less inclusion of Al in the geopolymeric network. The prism-shaped particles consisted of Na, C, O, and trace Al and Si, according to the EDX results (Fig. 6f). This particle was likely to be Na$_2$CO$_3$ crystalline, which would have a negative effect on the mechanical properties of geopolymer (He et al., 2013).

3.3.4. Pore analysis

Fig. 7 gives the pore size distribution and cumulative pore volume of the alkali-activation products, as determined by N$_2$ adsorption using the BJH method. One prominent characteristic pore size appeared as a clear peak centered at about 35 nm for all specimens. This mesopore can be attributed to the capillary pores derived from the space of geopolymeric gel units (Zhang et al., 2014). In addition, another smaller pore size of approximately 4 nm is evident for G-Hal$_{450}$, which was related to the intrinsic pores formed by hydrosodalite (Zhang et al., 2019).

Although G-Hal$_{650}$, G-Hal$_{750}$, and G-Hal$_{850}$ showed no conspicuous difference in XRD pattern (Fig. 4), the pore size distribution showed evident variation for G-Hal$_{650}$. As shown in Fig. 7b, the cumulative pore volume of G-Hal$_{650}$ was higher than for G-Hal$_{750}$ and G-Hal$_{850}$, which was one reason for its lower compressive strength. Notably, G-Hal$_{1000}$ had the fewest pores, but it did not have the highest compressive strength. Thus, it would appear there is no direct relationship between porosity and compressive strength, at least in the mesopore range.
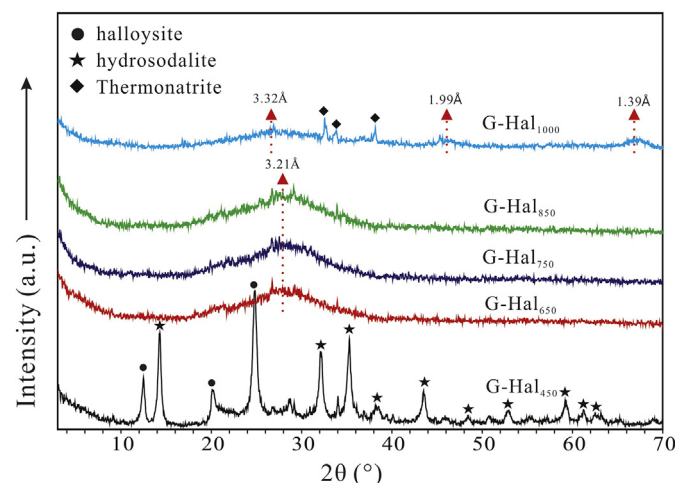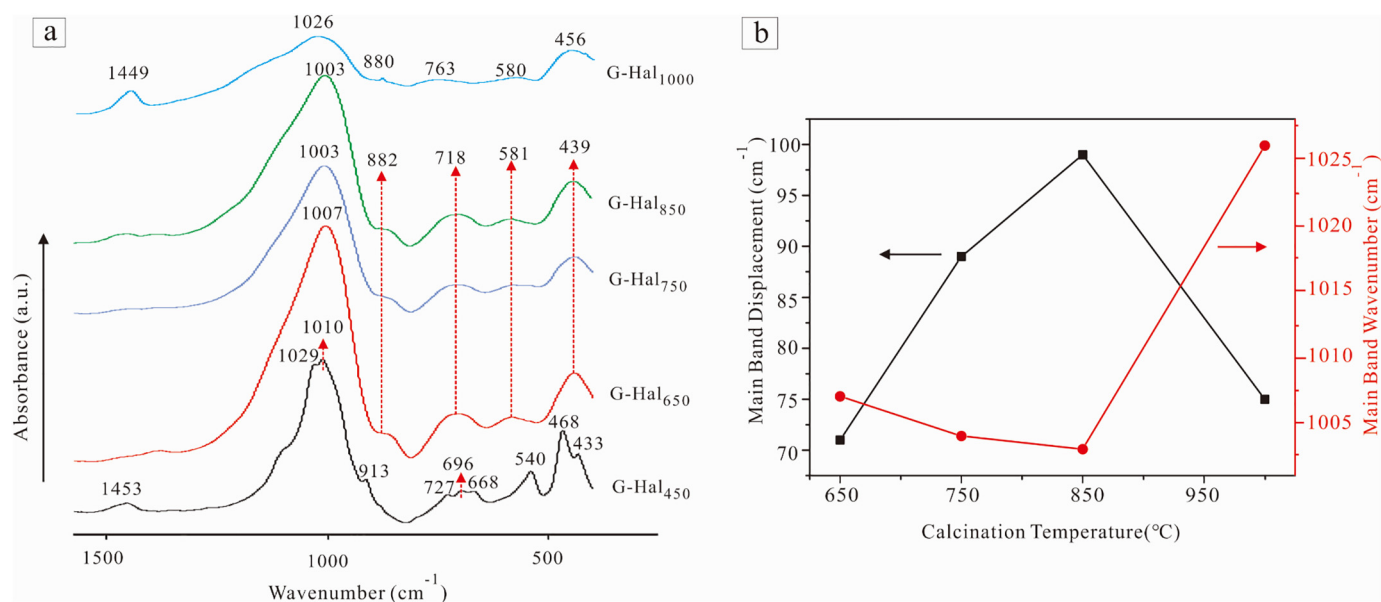

Fig. 4. XRD patterns of G-Hal$_T$.

Fig. 5. FTIR spectra of alkali-activation products (a) and the main band and its displacement for G-Hal$_T$ (b).
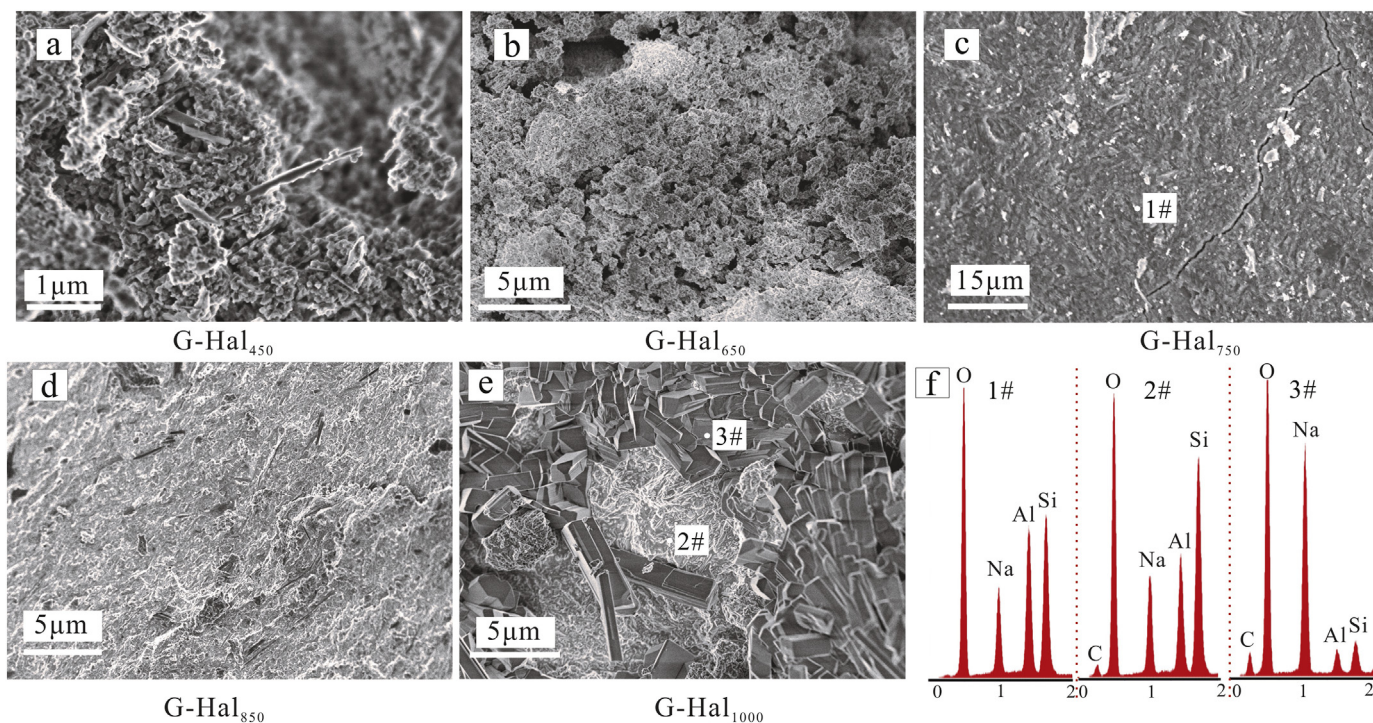

Fig. 6. SEM images of G-Hal$_T$ (a-e) and EDX analysis of selected points (f).

Indeed, the components of alkali-activation products made the main contribution to compressive strength gain. The higher degree of geopolymerization for G-Hal$_{750}$ and G-Hal$_{850}$ favored higher compressive strength, although they were more porous than G-Hal$_{450}$ and G-Hal$_{1000}$.

3.3.5. NMR results

The ^{27}Al MAS NMR spectrum for Hal$_{450}$ (Fig. 8a) showed a single resonance centered at 7 ppm, which was ascribed to octahedrally coordinated Al (Al^{VI}). When the calcination temperature was increased to 750 °C, the ^{27}Al MAS NMR spectrum showed three resonances centered at 7, 32, and 58 ppm, which were assigned to Al^{VI}, Al^V, and Al^{IV}, respectively. This demonstrated that an amorphous phase was formed (Wan et al., 2017a). The Al^V content decreased to zero, accompanied by

an increase of Al^{IV} (60 ppm) and Al^{VI} (10 ppm) when the calcination temperature was increased to 1000 °C. After mixing with alkaline solution, a resonance centered at 7 ppm still existed in G-Hal$_{450}$ but differed in relative intensity. A new resonance at 65 ppm appeared, which correlated to Al^{IV} and was characteristic of hydrosodalite (Marsh et al., 2018). The ^{27}Al MAS NMR spectrum of G-Hal$_{750}$ showed a strong resonance at 61 ppm with a rather weak resonance at about 7 ppm, revealing that the Al was mainly four-coordination (Al^{IV}) in the geopolymer sample. In the spectrum of G-Hal$_{1000}$, the resonances of Al^{IV} and Al^{VI} were still present. Based on semi-quantitative estimation, the Al^{IV}/Al^{VI} ratio increased from 0.41 to 1.30 after alkali-activation, which implied that partial Al^{VI} was transformed into Al^{IV} during geopolymerization.
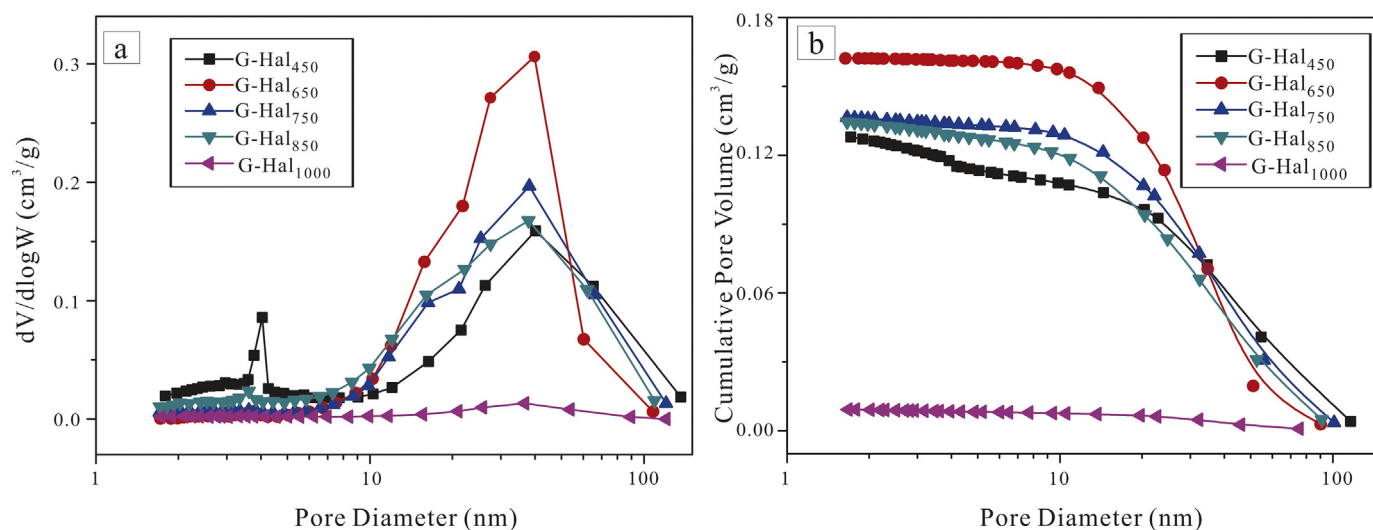
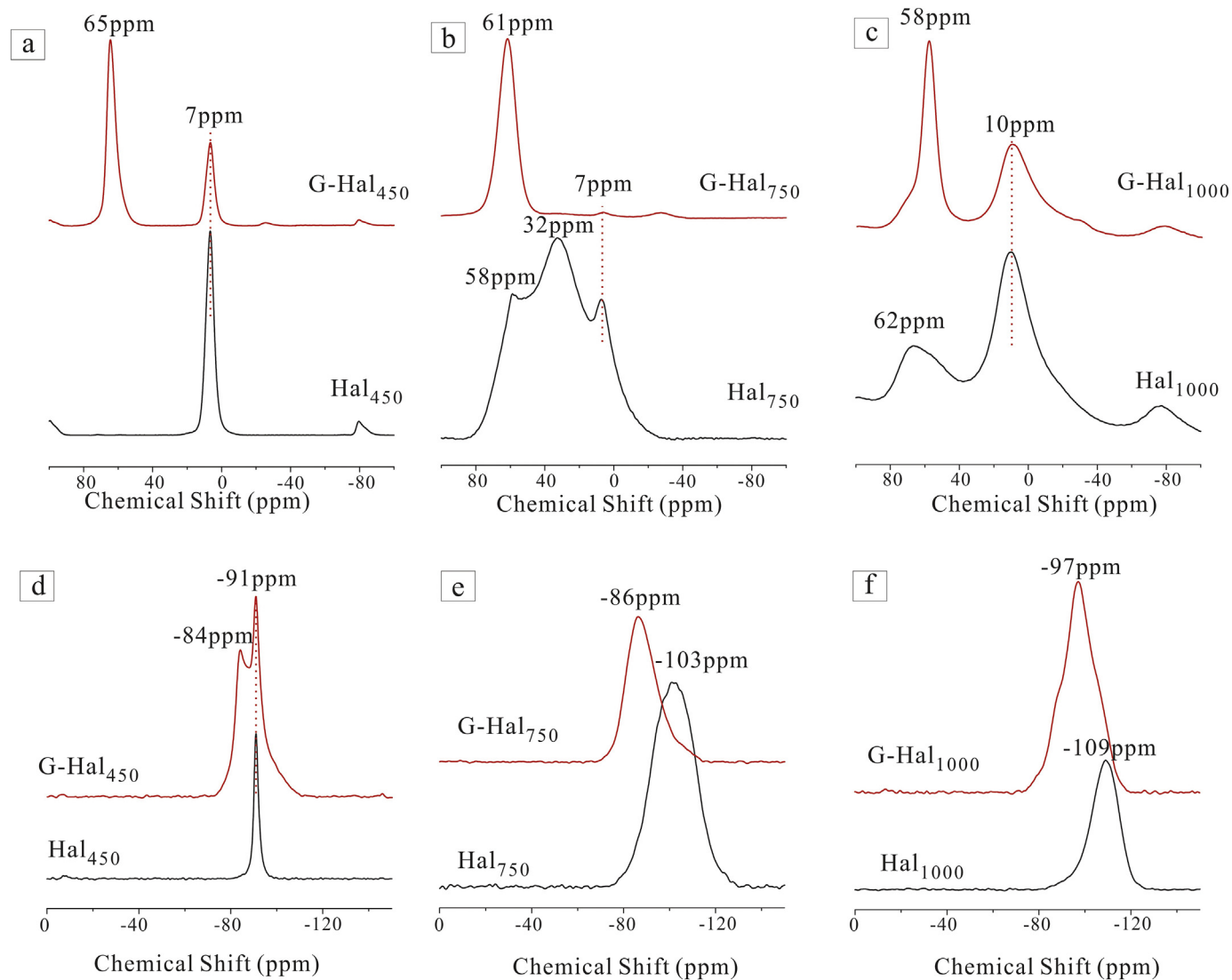**Fig. 7.** Pore size distribution (a) and cumulative pore volume (b) of Hal$_T$.

Fig. 8. ^{27}Al MAS NMR spectra of Hal$_T$ and G-Hal$_T$ (a, b, c) and ^{29}Si CP/MAS NMR spectra of Hal$_T$ and G-Hal$_T$ (d, e, f).
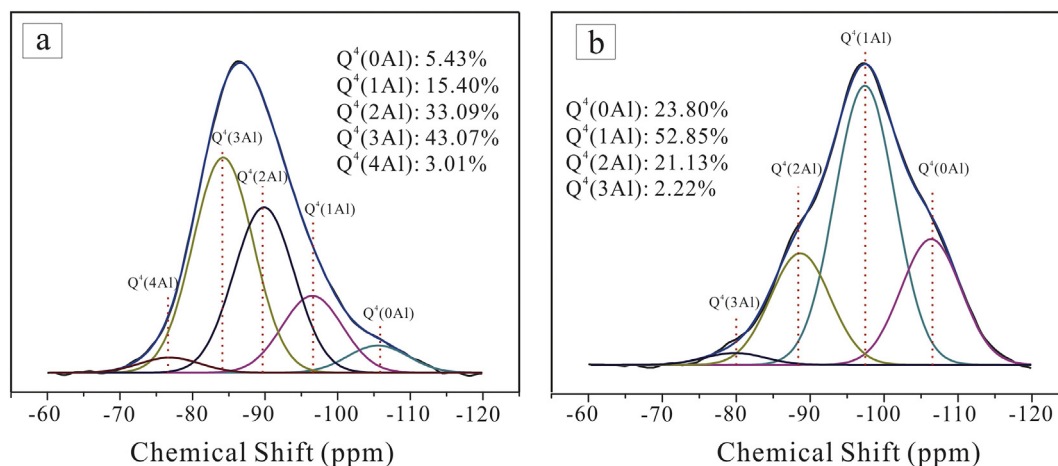
Fig. 9. Deconvolution of the ^{29}Si CP/MAS NMR spectrum of G-Hal$_{750}$ (a) and G-Hal$_{1000}$ (b).
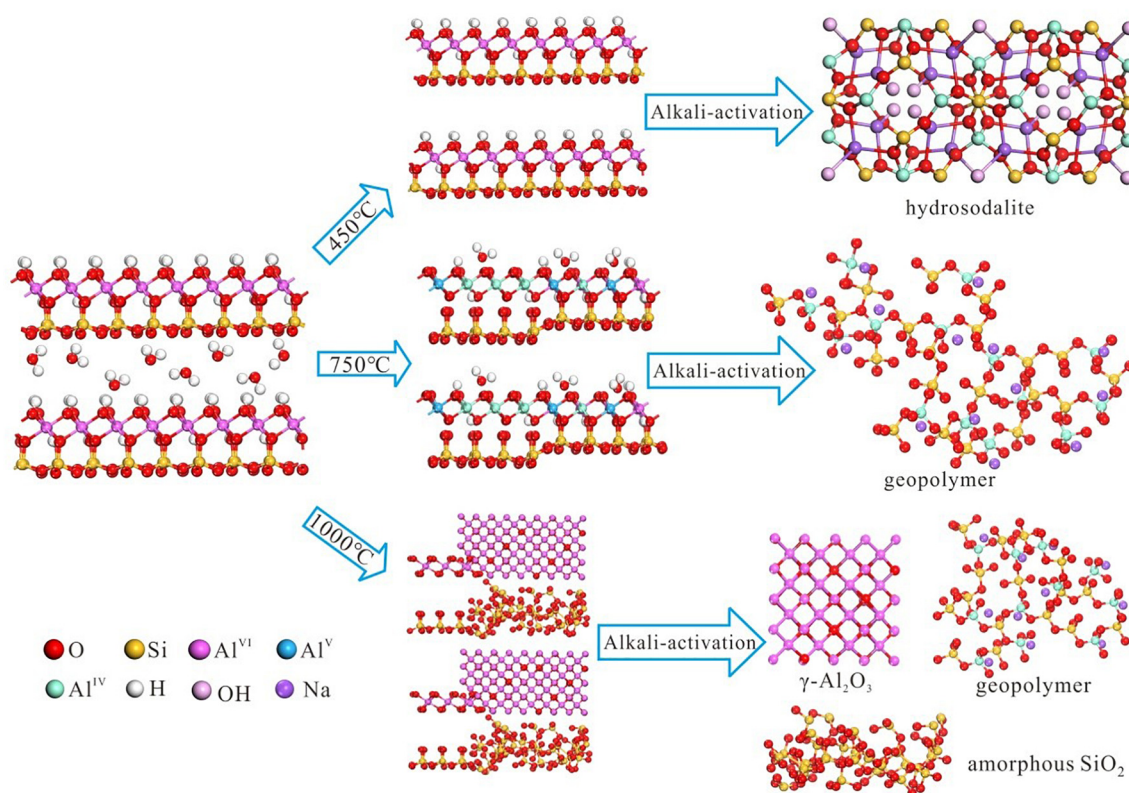

Fig. 10. Schematic diagram of structural changes in halloysite under different calcination temperatures and the corresponding alkali-activation products.

In the ^{29}Si CP/MAS NMR spectrum of Hal$_{450}$ (Fig. 8 d), one narrow resonance located at -91 ppm was assigned to Q^3(0Al) (Yan et al., 2017). This meant that calcination at low temperatures does not change the fundamental structure of halloysite, which was also evidenced by the ^{27}Al MAS NMR spectrum of Hal$_{450}$. As the calcination temperature was increased to 750 °C and 1000 °C, the resonances shifted to -103 and -109 ppm (Fig. 8b, c), which were assigned to Q^3 and Q^4, respectively (Mozgawa et al., 2002). After reaction with the alkaline solution, the new resonance centered at -84 ppm in the ^{29}Si CP/MAS NMR spectrum of G-Hal$_{450}$ was assigned to Q^4(4Al) bonding in the hydrosodalite framework (Klinowski, 1988). In addition, the presence of resonance at -91 ppm indicated unreacted halloysite. For G-Hal$_{750}$ and G-Hal$_{1000}$, it can be seen that the resonance center shifted to a higher field after geopolymerization. This change in the Si chemical environment correlated to the connection of tetrahedral [AlO$_4$] (Wilson

et al., 1986; Walkley and Provis, 2019).

To overcome the low spectral resolution for Si in geopolymers, Gaussian peak deconvolution was applied to separate and quantify Q^4(mAl) (0 ≤ m ≤ 4) species in NMR analysis. Deconvolution of the spectrum for G-Hal$_{750}$ produced five resonances centered at approximately -106, -97, -90, -85, and -78 ppm, which were attributed to Q^4(0Al), Q^4(1Al), Q^4(2Al), Q^4(3Al), and Q^4(4Al) (Xu et al., 2017). As shown in Fig. 9a, the percentages of Q^4(3Al) and Q^4(2Al) were the largest, at 43.07% and 33.09%, respectively. One tetrahedral [SiO$_4$] unit was mainly linked to two or three [AlO$_4$] units in this geopolymeric network. However, deconvolution of the spectrum for G-Hal$_{1000}$ only produced four resonances centered at approximately -106, -97, -90, and -80 ppm, which were attributed to Q^4(0Al), Q^4(1Al), Q^4(2Al), Q^4(3Al). The geopolymeric network of G-Hal$_{1000}$ was mainly composed of Q^4(1Al), at the 52.85% level (Fig. 9b). Therefore, one tetrahedral

[SiO$_4$] unit was mainly linked to one [AlO$_4$] unit for G-Hal$_{1000}$. In addition, Q^4(2Al) accounted for 21.13% and amorphous SiO$_2$ (Q^4(0Al)) accounted for 23.80%. This result suggests that less Al was included in the geopolymeric network of G-Hal$_{1000}$ compared with G-Hal$_{750}$ (Kränzlein et al., 2018), which was in agreement with the EDX result (Fig. 6f). This result also verifies the formation of higher geopolymeric gel contents for G-Hal$_{750}$ than G-Hal$_{1000}$.

3.4. The mechanism of alkali-activated calcined halloysite

The preceding results show that the calcination temperature of halloysite has an important effect on the microstructures and properties of resultant alkali-activation products. Halloysite retains its original tubular shape after thermal treatment even at 900 °C (Yuan et al., 2012). The inside and outside surfaces of the halloysite tube are both easily attacked by alkaline solution. At the same time, the high specific surface area of halloysite provides more contact with the alkaline solution. Therefore, calcined halloysite possesses higher geopolymerization reactivity than metakaolinite, including a higher dissolution rate of Si and Al, faster geopolymerization, and more rapid development of compressive strength (Zhang et al., 2012a).

As Fig. 10 illustrates, various structural changes occurred in halloysite when it was calcined at different temperatures. At a low temperature (450 °C), interlayer water and physical absorption water were removed but no other structural changes took place. The high degree of crystallinity resulted in low reactivity. The low dissolution rate of Si and Al meant that polycondensation was difficult to occur at ambient temperature, whereas the mixture paste hardened at elevated temperature showed low compressive strength because it consisted of unreacted halloysite and hydrosodalite rather than geopolymer. When the calcination temperature exceeded 650 °C, the hydrogen atoms and hydroxyl groups were separated from the Al-O-H bond to form H$_2$O molecules during dehydroxylation. Structural changes took place in the halloysite. The formation of amorphous SiO$_2$, four-coordination Al, and five-coordination Al were key factors in increasing pozzolanic activity (Fernandez et al., 2011; Fabbri et al., 2013; Garg and Skibsted, 2019). The matrix of G-Hal$_{750}$ was more homogeneous and compact (Fig. 6) because Hal$_{750}$ had sufficient dehydration and suitable setting time during geopolymerization. At the highest calcination temperature (1000 °C), γ-Al$_2$O$_3$ was formed locally, accompanied by the separation of amorphous Al$_2$O$_3$ and amorphous SiO$_2$ (Yuan et al., 2012). Although geopolymerization also took place in reaction to the silicate sodium solution, the microstructures of G-Hal$_{1000}$ differed from those of G-Hal$_{750}$. The reduced inclusion of Al in the geopolymer network caused a lower degree of geopolymerization. In addition to geopolymeric networks, G-Hal$_{1000}$ contained unreacted halloysite and silicate sodium, unreacted γ-Al$_2$O$_3$, amorphous SiO$_2$, and Na$_2$CO$_3$. As a result, G-Hal$_{1000}$ did not exhibit high strength even though it was dense and compact.

4. Conclusion

The performance of calcined halloysite in the preparation of alkali-based geopolymer was investigated in this study. The dependence of the microstructure and mechanical properties of the resultant alkali-based geopolymer on structural changes induced by the calcination of halloysite was outlined using a combination of microscopic and spectroscopic techniques. When calcined at 450 °C, the halloysite remained chemically stable and showed low reactivity with alkaline solution. The alkali-activation product was hydrosodalite with unreacted halloysite, which exhibited a porous structure with poor mechanical properties. When the halloysite was calcined between 650 °C and 850 °C, substantial changes occurred in its crystalline structure due to dehydroxylation. The leaching of Si and Al dissolved from the alkaline solution increased significantly. Consequently, a geopolymer network was formed for alkali-activation of halloysite calcined between 650 °C and 850 °C. The halloysite calcined at 750 °C and 850 °C possessed sufficient

reactivity with alkaline solution and formed a denser and more compact microstructure after geopolymerization than the halloysite calcined at 650 °C. Accordingly, alkali-activated calcined halloysite at 750 °C and 850 °C showed greater compressive strength. The compressive strength of the geopolymer decreased when the halloysite was calcined at 1000 °C. The formation of γ-Al$_2$O$_3$ reduced geopolymerization reactivity, because the amount of released Al was very small and thereby unfavorable for geopolymerization. These findings indicate that the properties and microstructures of halloysite-based geopolymer products and any related materials are greatly dependent on the microstructure of calcined halloysite. Careful thermal pretreatment of halloysite is useful for tailoring the performance of halloysite-based geopolymer materials.

Declaration of Competing Interest

None.

References

Heide, F., 2006. High temperature mass spectrometric gas-release studies of kaolinite Al$_2$[Si$_2$O$_5$(OH)$_4$] decomposition. Thermochim. Acta 446, 106–112.

Alkan, M., Hopa, C., Yilmaz, Z., Güler, H., 2005. The effect of alkali concentration and solid/liquid ratio on the hydrothermal synthesis of zeolite NaA from natural kaolinite. Microporous Mesoporous Mater. 86, 176–184.

Barrie, E., Cappuyns, V., Vassilieva, E., Adriaens, R., Hollanders, S., Garcés, D., Paredes, C., Pontikes, Y., Elsen, J., Machiels, L., 2015. Potential of inorganic polymers (geopolymers) made of halloysite and volcanic glass for the immobilisation of tailings from gold extraction in Ecuador. Appl. Clay Sci. 109-110, 95–106.

Belmokhtar, N., El Ayadi, H., Ammari, M., Ben Allal, L., 2018. Effect of structural and textural properties of a ceramic industrial sludge and kaolin on the hardened geopolymer properties. Appl. Clay Sci. 162, 1–9.

Buchwald, A., Hohmann, M., Posern, K., Brendler, E., 2009. The suitability of thermally activated illite/smectite clay as raw material for geopolymer binders. Appl. Clay Sci. 46, 300–304.

Bumanis, G., Novais, R.M., Carvalheiras, J., Bajare, D., Labrincha, J.A., 2019. Metals removal from aqueous solutions by tailored porous waste-based granulated alkali-activated materials. Appl. Clay Sci. 179 (9).

Deng, L., Yuan, P., Liu, D., Annabi-Bergaya, F., Zhou, J., Chen, F., 2017. Effects of microstructure of clay minerals, montmorillonite, kaolinite and halloysite, on their benzene adsorption behaviors. Appl. Clay Sci. 143, 184–191.

Dietel, J., Warr, L., Bertmer, M., Steudel, A., Grathoff, G.H., Emmerich, K., 2017. The importance of specific surface area in the geopolymerization of heated illitic clay. Appl. Clay Sci. 139, 99–107.

Duan, P., Yan, C., Zhou, W., 2017. Compressive strength and microstructure of fly ash based geopolymer blended with silica fume under thermal cycle. Cem. Concr. Compos. 78, 108–119.

Duxson, P., Fernández-Jiménez, A., Provis, J., Lukey, G., Palomo, A., Deventer, J., 2007. Geopolymer technology: the current state of the art. J. Mater. Sci. 42, 2917–2933.

Elimbi, A., Tchakoute, H., Njopwouo, D., 2011. Effects of calcination temperature of kaolinite clays on the properties of geopolymer cements. Constr. Build. Mater. 25, 2805–2812.

Fabbri, B., Gualtieri, S., Leonardi, C., 2013. Modifications induced by the thermal treatment of kaolin and determination of reactivity of metakaolin. Appl. Clay Sci. 73, 2–10.

Farzadnia, N., Ali, A., Demirboga, R., Anwar, M., 2013. Effect of halloysite nanoclay on mechanical properties, thermal behavior and microstructure of cement mortars. Cem. Concr. Res. 48, 97–104.

Fernandez, R., Martirena, F., Scrivener, K.L., 2011. The origin of the pozzolanic activity of calcined clay minerals: a comparison between kaolinite, illite and montmorillonite. Cem. Concr. Res. 41, 113–122.

Ferone, C., Liguori, B., Capasso, I., Colangelo, F., Cioffi, R., Cappelletto, E., Di Maggio, R., 2015. Thermally treated clay sediments as geopolymer source material. Appl. Clay Sci. 107, 195–204.

Font, A., Borrachero, M., Soriano, L., Monzo, J., Mellado, A., Paya, J., 2018. New eco-cellular concretes: sustainable and energy-efficient materials. Green Chem. 20,

4684–4694.

Frost, R., Vassallo, A., 1996. The dehydroxylation of the kaolinite clay minerals using infrared emission spectroscopy. Clay Clay Miner. 44, 635–651.

Gao, K., Lin, K., Wang, D., Hwang, C., Shiu, H., Chang, Y., Cheng, T., 2014. Effects SiO_2/Na_2O molar ratio on mechanical properties and the microstructure of nano-SiO_2 metakaolin-based geopolymers. Constr. Build. Mater. 53, 503–510.

Garg, N., Skibsted, J., 2019. Dissolution kinetics of calcined kaolinite and montmor-illonite in alkaline conditions: evidence for reactive Al(V) sites. J. Am. Ceram. Soc. 102 (12), 7720–7734.

Hanjitsuwan, S., Hunpratub, S., Thongbai, P., Maensiri, S., Sata, V., Chindaprasirt, P., 2014. Effects of NaOH concentrations on physical and electrical properties of high calcium fly ash geopolymer paste. Cem. Concr. Compos. 45, 9–14.

He, J., Jie, Y., Zhang, J., Yu, Y., Zhang, G., 2013. Synthesis and characterization of red mud and rice husk ash-based geopolymer composites. Cem. Concr. Compos. 37, 108–118.

Hollanders, S., Adriaens, R., Skibsted, J., Cizer, Ö., Elsen, J., 2016. Pozzolanic reactivity of pure calcined clays. Appl. Clay Sci. 132-133, 552–560.

Hounsi, A., Lecomte, G., 2013. Kaolin-based geopolymers: effect of mechanical activation and curing process. Constr. Build. Mater. 42, 105–113.

Hu, N., Bernsmeier, D., Grathoff, G., Warr, L., 2016. The influence of alkali activator type, curing temperature and gibbsite on the geopolymerization of an interstratified illite-smectite rich clay from Friedland. Appl. Clay Sci. 135, 386–393.

Joussein, E., 2016. Geology and mineralogy of nanosized tubular halloysite. In: Yuan, P., Thill, A., Bergaya, F. (Eds.), Nanosized Tubular Clay Minerals Halloysite and Imogolite. Developments in Clay Science 7. Elsevier, Amsterdam, pp. 12–48.

Joussein, E., Petit, S., Churchman, J., Theng, B., Righi, D., Delvaux, B., 2005. Halloysite clay minerals - a review. Clay Miner. 40, 383–426.

Joussein, E., Soubrand, M., Pascaud, G., Cogulet, A., Rossignol, S., 2019. Immobilization of Pb from mine sediments in metakaolin-based geomaterials. Environ. Sci. Pollut. Res. 26, 14473–14482.

Kani, E., Allahverdi, A., Provis, J., 2012. Efflorescence control in geopolymer binders based on natural pozzolan. Cem. Concr. Compos. 34, 25–33.

Kaze, C., Tchakoute, H., Mbakop, T., Mache, J., Kamseu, E., Melo, U., Leonelli, C., Rahier, H., 2018. Synthesis and properties of inorganic polymers (geopolymers) derived from Cameroon-meta-halloysite. Ceram. Int. 44, 18499–18508.

Khan, B., Ullah, M., 2004. Effect of a retarding admixture on the setting time of cement pastes in hot weather. J. King Saud Univ., Eng. Sci. 15, 63–79.

Klinowski, J., 1988. Recent advances in solid-state NMR of zeolites. Annu. Rev. Mater. Sci. 18, 189–218.

Kljajević, L., Nenadović, S., Nenadović, M., Bundaleski, N., Todorović, B., Pavlović, V., Rakočević, Z., 2017. Structural and chemical properties of thermally treated geopo-lymer samples. Ceram. Int. 43, 6700–6708.

Kouamo, H., Rüscher, C., 2017. Mechanical and microstructural properties of metakaolin-based geopolymer cements from sodium waterglass and phosphoric acid solution as hardeners: a comparative study. Appl. Clay Sci. 140, 81–87.

Kränzlein, E., Pöllmann, H., Krcmar, W., 2018. Metal powders as foaming agents in fly ash based geopolymer synthesis and their impact on the structure depending on the Na/Al ratio. Cem. Concr. Compos. 90, 161–168.

Lee, W., Deventer, J., 2003. Use of infrared spectroscopy to study geopolymerization of heterogeneous amorphous aluminosilicates. Langmuir. 19, 8726–8734.

Li, Z., Zhang, S., Zuo, Y., Chen, W., Ye, G., 2019. Chemical deformation of metakaolin based geopolymer. Cem. Concr. Res. 120, 108–118.

Liew, Y., Heah, C., Al Bakri, M., Hussin, K., 2016. Structure and properties of clay-based geopolymer cements: a review. Prog. Mater. Sci. 83, 595–629.

Marsh, A., Heath, A., Patureau, P., Evernden, M., Walker, P., 2018. A mild conditions synthesis route to produce hydrosodalite from kaolinite, compatible with extrusion processing. Microporous Mesoporous Mater. 264, 125–132.

Marsh, A., Heath, A., Patureau, P., Evernden, M., Walker, P., 2019. Phase formation behaviour in alkali activation of clay mixtures. Appl. Clay Sci. 175, 10–21.

Mclellan, B., Williams, R., Lay, J., Riessen, A., Corder, G., 2011. Costs and carbon emissions for geopolymer pastes in comparison to ordinary portland cement. J. Clean. Prod. 19, 1080–1090.

Monneron-Gyurits, M., Joussein, E., Soubrand, M., Fondaneche, P., Rossignol, S., 2018. Valorization of mussel and oyster shells toward metakaolin-based alkaline activated material. Appl. Clay Sci. 162, 15–26.

Mozgawa, W., Fojud, Z., Handke, M., Jurga, S., 2002. MAS NMR and FTIR spectra of framework aluminosilicates. J. Mol. Struct. 614, 281–287.

Owsiak, Z., Soltys, A., 2015. The influence of a halloysite additive on the performance of autoclaved aerated concrete. Ceram.-Silik. 59, 24–28.

Prokof'ev, V., Gordina, N., 2014. Preparation of granulated LTA and SOD zeolites from mechanically activated mixtures of metakaolin and sodium hydroxide. Appl. Clay Sci. 101, 44–51.

Provis, J., Bernal, S., 2014. Geopolymers and related alkali-activated materials. Annu. Rev. Mater. Res. 44 (1), 299–327.

Rees, C., Provis, J., Lukey, G., Deventer, J., 2007. Attenuated total reflectance fourier transform infrared analysis of fly ash geopolymer gel aging. Langmuir. 23, 8170–8179.

Ribeiro, R., Ribeiro, M., Sankar, K., Kriven, W., 2016. Geopolymer-bamboo composite – a novel sustainable construction material. Constr. Build. Mater. 123, 501–507.

Selmani, S., Sdiri, A., Bouaziz, S., Joussein, E., Rossignol, S., 2017. Effects of metakaolin addition on geopolymer prepared from natural kaolinitic clay. Appl. Clay Sci. 146, 446–457.

Shi, C., Jiménez, F., Palomo, A., 2011. New cements for the 21st century: the pursuit of an alternative to Portland cement. Cem. Concr. Res. 41 (7), 750–763.

Tchadjie, L., Ekolu, S., 2018. Enhancing the reactivity of aluminosilicate materials toward geopolymer synthesis. J. Mater. Sci. 53, 4709–4733.

Tchakouté, H., Kamseu, E., Banenzoué, C., Rüscher, C., Andreola, F., Tchamo, C., Leonelli, C., 2018. Role of γ-Al_2O_3 on the mechanical and microstructural properties of metakaolin-based geopolymer cements. J. Sol-Gel Sci. Tech. 86, 305–315.

Temuujin, J., Minjigmaa, A., Rickard, W., Lee, M., Williams, I., Riessen, A.V., 2009. Preparation of metakaolin based geopolymer coatings on metal substrates as thermal barriers. Appl. Clay Sci. 46, 265–270.

Walkley, B., Provis, J., 2019. Solid-state nuclear magnetic resonance spectroscopy of cements. Materialstoday Advances 1, 100007.

Wan, Q., Rao, F., Song, S., 2017a. Reexamining calcination of kaolinite for the synthesis of metakaolin geopolymers - roles of dehydroxylation and recrystallization. J. Non-Cryst. Solids 460, 74–80.

Wan, Q., Rao, F., Song, S., García, R., Estrella, R., Patiño, C., Zhang, Y., 2017b. Geopolymerization reaction, microstructure and simulation of metakaolin-based geopolymers at extended Si/Al ratios. Cem. Concr. Compos. 79, 45–52.

Wei, Y., Yuan, P., Liu, D., Losic, D., Tan, D., Chen, F., Liu, H., Du, P., Zhou, J., 2019. Activation of natural halloysite nanotubes by introducing lanthanum oxycarbonate nanoparticles via co-calcination for outstanding phosphate removal. Chem. Commun. 55, 2110–2113.

White, C., Provis, J., Proffen, T., Riley, D., Deventer, J., 2010. Density functional mod-eling of the local structure of kaolinite subjected to thermal dehydroxylation. J. Phys. Chem. A 114, 4988–4996.

White, R., Bavykin, D., Walsh, F., 2012. The stability of halloysite nanotubes in acidic and alkaline aqueous suspensions. Nanotechnology. 23, 065705.

Wilson, M., McCarthy, S., Fredericks, P., 1986. Structure of poorly-ordered aluminosili-cates. Clay Miner. 21, 879–897.

Xu, C., Sutrisno, A., Struble, L., Xu, C., Sutrisno, A., Struble, L., 2017. Effects of calcium on setting mechanism of metakaolin-based geopolymer. J. Am. Ceram. Soc. 101.

Yan, K., Guo, Y., Fang, L., Cui, L., Cheng, F., Li, T., 2017. Decomposition and phase transformation mechanism of kaolinite calcined with sodium carbonate. Appl. Clay Sci. 147, 90–96.

Yuan, P., 2016. Thermal-treatment-induced deformations and modifications of halloysite. In: Yuan, P., Thill, A., Bergaya, F. (Eds.), Nanosized Tubular Clay Minerals Halloysite and Imogolite. Developments in Clay Science 7. Elsevier, Amsterdam, pp. 137–166.

Yuan, P., Yang, D., Lin, Z., He, H., Wen, X., Wang, L., Deng, F., 2006. Influences of pretreatment temperature on the surface silylation of diatomaceous amorphous silica with trimethylchlorosilane. J. Non-Cryst. Solids 352, 3762–3771.

Yuan, P., Southon, P., Liu, Z., Mer, G., Hook, J., Antill, S.J., Kepert, C., 2008. Functionalization of halloysite clay nanotubes by grafting with γ-aminopropyl-triethoxysilane. J. Phys. Chem. C 112 (40), 15742–15751.

Yuan, P., Tan, D., Aannabi-Bergaya, F., Yan, W., Fan, M., Liu, D., He, H., 2012. Changes in structure, morphology, porosity, and surface activity of mesoporous halloysite na-notubes under heating. Clay Clay Miner. 60, 561–573.

Yuan, P., Tan, D., Annabi-Bergaya, F., 2015. Properties and applications of halloysite nanotubes: recent research advances and future prospects. Appl. Clay Sci. 112, 75–93.

Yuan, J., He, P., Jia, D., Yang, C., Zhang, Y., Yan, S., Yang, Z., Duan, X., Wang, S., Zhou, Y., 2016. Effect of curing temperature and SiO_2/K_2O molar ratio on the performance of metakaolin-based geopolymers. Ceram. Int. 42, 16184–16190.

Zapala-Slaweta, J., 2017. The effect of meta-halloysite on alkali-aggregate reaction in concrete. Mater. Struct. 50, 217.

Zhang, Z., Yao, X., Zhu, H., Hua, S., Chen, Y., 2009a. Activating process of geopolymer source material: kaolinite. J. Wuhan. Univ. Technol. 24, 132–136.

Zhang, Z., Xiao, Y., Huajun, Z., Yue, C., 2009b. Role of water in the synthesis of calcined kaolin-based geopolymer. Appl. Clay Sci. 43, 218–223.

Zhang, Z., Wang, H., Yao, X., Zhu, Y., 2012a. Effects of halloysite in kaolin on the for-mation and properties of geopolymers. Cem. Concr. Compos. 34, 709–715.

Zhang, Z., Wang, H., Provis, J., Bullen, F., Reid, A., Zhu, Y., 2012b. Quantitative kinetic and structural analysis of geopolymers. Part 1. The activation of metakaolin with sodium hydroxide. Thermochim. Acta 539, 23–33.

Zhang, Z., Provis, J., Wang, H., Bullen, F., Reid, A., 2013. Quantitative kinetic and structural analysis of geopolymers. Part 2. Thermodynamics of sodium silicate acti-vation of metakaolin. Thermochim. Acta 565, 163–171.

Zhang, Z., Wang, H., Zhu, Y., Reid, A., Provis, J., Bullen, F., 2014. Using fly ash to par-tially substitute metakaolin in geopolymer synthesis. Appl. Clay Sci. 88–89, 194–201.

Zhang, Z., Provis, J., Reid, A., Wang, H., 2015. Mechanical, thermal insulation, thermal resistance and acoustic absorption properties of geopolymer foam concrete. Cem. Concr. Compos. 62, 97–105.

Zhang, Z., Zhu, H., Zhou, C., Wang, H., 2016. Geopolymer from kaolin in China: an overview. Appl. Clay Sci. 119, 31–41.

Zhang, Z., Zhu, Y., Zhu, H., Zhang, Y., Provis, J., Wang, H., 2019. Effect of drying pro-cedures on pore structure and phase evolution of alkali-activated cements. Cem. Concr. Compos. 96, 194–203.